Vertical Transportation of Lunar Regolith and Ice Particles Using Vibrating Tube

Hiroyuki Kawamoto[1]; Keita Kubo[2]; Ryo Kikumiya[3]; and Masato Adachi[4]

Abstract: The Japan Aerospace Exploration Agency is planning to operate an uncrewed rover on the Moon to search for water ice, which exists at the polar regions of the Moon. The rover's 1.5-m-long drill will penetrate the regolith layer of the lunar surface and capture ice particles mixed with the regolith. A transportation system for crushed ice particles mixed with the lunar regolith has been developed utilizing a vibration transportation mechanism that realizes the lifting of particles to physical and chemical analyzers installed on the rover. In this mechanism, the friction force between the inner wall of the tube and particles mainly plays the role of conveying particles upward while the tube inserted vertically into the bulk of the regolith is oscillating up and down. A parametric experiment was conducted to deduce the optimal configuration and operational conditions, and it was achieved that simulant particles and crushed ice particles mixed with lunar regolith are transported through the long tube. In addition, it was predicted by numerical calculations based on the discrete element method that the transportation performance in the lunar environment is better than that on Earth owing to low gravitational acceleration on the Moon.
DOI: 10.1061/(ASCE)AS.1943-5525.0001346.

Author keywords: Lunar exploration; In situ resource utilization; Sampling; Ice; Regolith; Vibration transportation.

Introduction

Recent lunar explorations have revealed that water ice could exist at the polar regions of the Moon (Lucey 2009; Colaprete et al. 2010; Sanin et al. 2017; Li et al. 2018). Water is expected to be utilized to maintain life support for astronauts and provide a raw material for hydrogen and oxygen for fuel cells and rocket engines (Sanders and Larson 2011, 2013; Lee et al. 2013). Because the exact location of ice, its depth from the lunar surface, volume, and physical and chemical forms are not clear, the Japan Aerospace Exploration Agency (JAXA) is planning to search for ice directly by operating uncrewed rovers on the Moon. The rover being developed by JAXA will employ a 1.5-m-long drill for sampling, as shown in Fig. 1 (Hoshino et al. 2019; Wakabayashi et al. 2019). This rover will screw the drill vertically into the regolith layer, allowing ice mixed with regolith to be collected and lifted from the inferior portion of the regolith layer to the physical and chemical analyzers installed on the rover. A long-range vertical transportation technology of ice and regolith particles is indispensable to realize this process.

Several mechanical methods have been developed to sample regolith on the Moon and Mars. These methods include: drills in Luna 16, 20, and 24 missions (Zacny et al. 2013); a scoop, tong, and rake in Apollo missions (Allton 2009); scoops in Viking Lander 1 and 2 missions (Klein et al. 1976); the Icy Soil Acquisition Device (Honeybee Robotics Spacecraft Mechanisms, New York), which is composed of a scoop with passive cutting blades and a small motor-driven drill in the Phoenix Lander (Bonitz et al. 2009); and a scoop and drill in the Curiosity Rover (Abbey et al. 2019). These mechanical sampling methods have been successful on the Moon and Mars; however, they faced disadvantages such as high malfunction risks because of their complex structure, the needs of large mass and high power, mechanical abrasion caused by lunar regolith, and the complexity of their operation owing to communication delay. One of the authors has developed alternate sampling systems that utilize electrostatic force (Kawamoto and Shirai 2012; Kawamoto 2014; Kawamoto et al. 2016; Kawamoto and Yoshida 2018, Kawamoto et al. 2021). The proposed systems are simple, consume less power than conventional mechanical methods, and have no mechanically moving parts, thus making them less susceptible to mechanical and operational failures. One of these electrostatic systems can lift regolith and ice particles up to 1 m in height (Kawamoto et al. 2021).

In this study, another optional method was developed using a vibration transportation mechanism that is feasible for transporting particles to high positions (Akiyama and Shimomura 1991; Liu et al. 2013; Zhang et al. 2017). In this mechanism, the friction force between the inner wall of the tube and the sample mainly plays the role of conveying regolith particles upward while the tube inserted vertically into the regolith layer is oscillating in up and down. This novel phenomenon was first reported by Akiyama and Shimomura (1991) and called "surface level migration" by Ohtsuki (1998). In this study, a parametric experiment was conducted to deduce the optimal configuration and operational conditions, and it was demonstrated that crushed ice particles mixed with lunar regolith simulant, as well as the simulant regolith particles, are lifted for a long distance by optimizing the system configuration and its operational conditions. Moreover, the effect of gravity variation on the performance of this transportation system was investigated by performing a numerical calculation based on the discrete-element method (DEM) to predict its successful operation on the Moon.

[1]Researcher Emeritus, Research Institute for Science and Engineering, Waseda Univ., 17, Kikuicho, Shinjuku, Tokyo 162-0044, Japan (corresponding author). Email: kawa@waseda.jp

[2]Student, Dept. of Applied Mechanics and Aerospace Engineering, Waseda Univ., 3-4-1, Okubo, Shinjuku, Tokyo 169-8555, Japan. Email: mkr19090@ruri.waseda.jp

[3]Student, Dept. of Applied Mechanics and Aerospace Engineering, Waseda Univ., 3-4-1, Okubo, Shinjuku, Tokyo 169-8555, Japan. Email: kikumiya0516@ruri.waseda.jp

[4]Reserecher, Institut für Materialphysik im Weltraum, Deutsches Zentrum für Luft- und Raumfahrt (DLR), Köln 51170, Germany. Email: Masato.Adachi@dlr.de

Note. This manuscript was submitted on July 25, 2020; approved on July 6, 2021; published online on August 25, 2021. Discussion period open until January 25, 2022; separate discussions must be submitted for individual papers. This paper is part of the ***Journal of Aerospace Engineering***, © ASCE, ISSN 0893-1321.

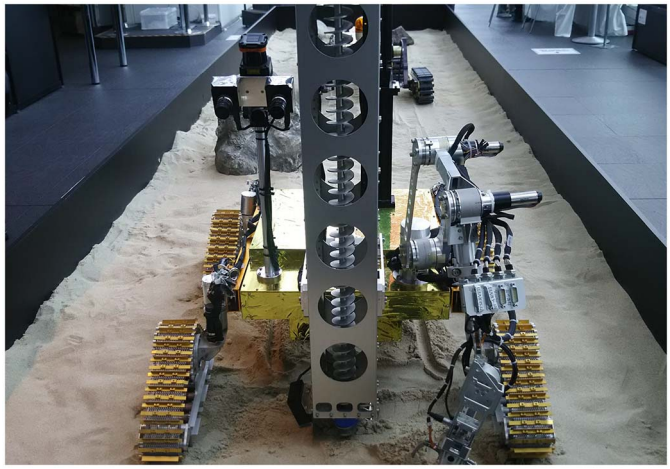

Fig. 1. Lunar rover for underground exploration developed by JAXA. Physical and chemical analyses will be made using samples acquired when excavating up to 1.5 m deep using a drill installed at the middle of the rover. (Image by Hiroyuki Kawamoto.)

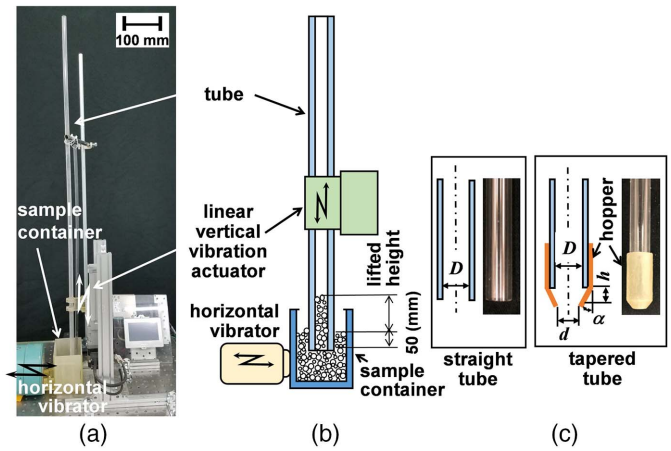

Fig. 2. Experimental apparatus: (a) photograph; (b) schematic illustration of the proposed system; and (c) lower end shapes of tubes.

System Configuration

A photograph of the proposed system and its schematic illustration of the system are shown in Figs. 2(a and b), respectively. This system consists of a transportation tube and a vertical linear vibration actuator. The tube was inserted into the bulk layer of regolith at a depth of 50 mm (Zhang et al. 2017, 2018). Sample particles in a container (W100 × D80 × L110 mm) were lifted upward through the vertically supported tube made of transparent acrylic resin. The experimental parameter set for the tube was its inner diameter of the tube, denoted by D; the tube had a thickness of 1 mm and length of 1 m. In addition to the straight tube, a tapered tube was prepared (Liu et al. 2014). A hopper was attached at the lower end of the straight tube to form the tapered tube, as shown in Fig. 2(c).

The inner diameter d and tilt angle α of the hopper tip were the experimental parameters for the tapered tube. The tube was vibrated vertically using a linear vibration actuator (EZS3-D005-AZAAD-1, Oriental Motor, Tokyo). The container was horizontally vibrated with an amplitude of 0.1 mm and a frequency of 50 Hz (1g) using an electromagnetic vibrator (G21-005D, Shinken, Tokyo) to break apart agglutinated particles in the container. A preliminary experiment indicated that the frequency of the horizontal vibration did not significantly affect the lifting performance. Although the application of horizontal vibration assists the stable capture of particles, it is unnecessary for specific conditions. The operation of the horizontal vibrator was also a parameter for the experiment.

The glass beads, lunar regolith simulant, and ice particles shown in Fig. 3 were used as the samples in the experiments. Three types of soda-lime glass beads (Fuji Manufacturing, Tokyo) were used to investigate the fundamental characteristics of this system, because they are spherical and uniform as shown in Fig. 3(c). They are FGB-180 (106–90 μm in diameter and 22° repose angle), B-240 (75–63 μm in diameter and 25° repose angle), and FG320 (53–38 μm in diameter and 30° repose angle). The specific gravity of the beads was 2.5. Lunar regolith simulant (FJS-1, Shimizu Corp., Tokyo) (Kanamori et al. 1998) shown in Fig. 3(b), which is similar to the well-known simulant JSC1-A (McKay et al. 1991), was used because lunar ice particles are expected to be scattered in lunar regolith.

Ice particles were generated from frozen tap water mixed with the lunar regolith simulant, which was crushed and sieved through a 212-μm mesh. The experiment was conducted in an air-conditioned laboratory (20°C–25°C and 40%–60% relative humidity) for the glass beads and lunar regolith simulant, whereas the experiment for ice particles was carried out in a freezer (−35°C) (NF-75SF3, Nihon Freezer, Tokyo) at atmospheric pressure. It has been reported that interstitial air can influence the lifting velocity of particles; however, it is not a prerequisite to lift particles (Liu et al. 2013). The present results conducted at atmospheric pressure would be valid in a vacuum. The effect of gravity is investigated numerically in the following section to confirm the effectiveness of the system on the Moon.

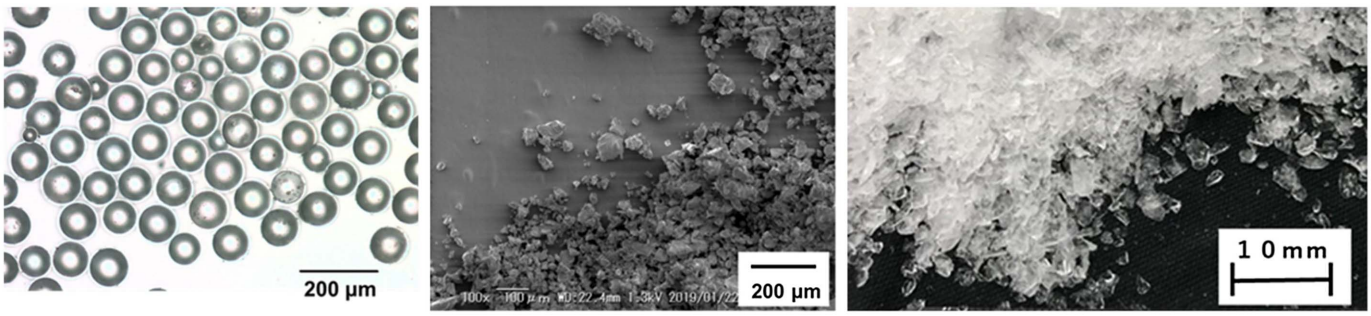

Fig. 3. Particles used in experiments: (a) glass beads; (b) lunar regolith simulant; and (c) crashed water ice.

Numerical Calculation

To predict the effects of gravity on the performance of this transportation system, a numerical calculation based on the three-dimensional DEM was performed using open-source LIGGGHTS version 3.8.0 software (Cundall and Strack 1979; Kloss et al. 2012). The motion equation for the ith particle is represented by Eqs. (1) and (2)

$$m_i \frac{d\boldsymbol{v_i}}{dt} = \sum_{j=1}^{n} (\boldsymbol{F_{nij}} + \boldsymbol{F_{tij}}) + m_i \boldsymbol{g} \tag{1}$$

$$I_i \frac{d\boldsymbol{\omega_i}}{dt} = \sum_{j=1}^{n} (\boldsymbol{M_{ij}} + \boldsymbol{M_{rij}}) \tag{2}$$

where $m_i, I_i, \boldsymbol{v_i}, \boldsymbol{\omega_i}$, n, and $\boldsymbol{g}$ = particle's mass, moment of inertia, translational and angular velocities, total number of particles in contact with particle i, and gravitational acceleration, respectively. The trajectory of the particle can be obtained by solving Eqs. (1) and (2) with a small time-step repeatedly. $\boldsymbol{F_{nij}}$ and $\boldsymbol{F_{tij}}$ = normal and tangential components of the contact force between particles i and j, which can be described by Eqs. (3) and (4), respectively, These equations are derived from the Hertz contact theory and Mindlin contact theory

$$\boldsymbol{F_{nij}} = -k_{nij}\delta_{nij}\boldsymbol{n_{ij}} - c_{nij}\boldsymbol{v_{nij}} \tag{3}$$

$$\boldsymbol{F_{tij}} = -\min(\mu|\boldsymbol{F_{nij}}|\boldsymbol{t_{ij}}, k_{tij}\delta_{tij}\boldsymbol{t_{ij}} + c_{tij}\boldsymbol{v_{tij}}) \tag{4}$$

where k_{nji} and k_{tij} = normal and tangential spring constants; c_{nji} and c_{tij} = normal and tangential damping constants; δ_{nji} and δ_{tij} = normal and tangential overlaps between particles i and j; $\boldsymbol{n_{ij}}$ is the normal unit vector from particle i to j; $\boldsymbol{t_{ij}}$ is the tangential unit vector to $\boldsymbol{n_{ij}}$; $\boldsymbol{v_{nij}}$ and $\boldsymbol{v_{tij}}$ = normal and tangential relative velocities between particles i and j; and μ = particle's friction coefficient, respectively. If a slip occurs when the particles are in contact, the frictional force limits the tangential force. The spring and damping constants are calculated using Eqs. (5)–(8)

$$k_{nij} = \frac{4}{3}\sqrt{\frac{r_i r_j}{r_i + r_j}\delta_{nij}}\left(\frac{1-\nu_i^2}{E_i} + \frac{1-\nu_j^2}{E_j}\right)^{-1} \tag{5}$$

$$c_{nij} = -\frac{\ln(\varepsilon)}{\sqrt{(\ln^2(\varepsilon) + \pi^2)}}\sqrt{5k_{nij}\frac{m_i m_j}{m_i + m_j}} \tag{6}$$

$$k_{tij} = 8\sqrt{\frac{r_i r_j}{r_i + r_j}\delta_{nij}}\left(\frac{2-\nu_i^2}{G_i} + \frac{2-\nu_j^2}{G_j}\right)^{-1} \tag{7}$$

$$c_{tij} = -\frac{\ln(\varepsilon)}{\sqrt{(\ln^2(\varepsilon) + \pi^2)}}\sqrt{\frac{10}{3}k_{tij}\frac{m_i m_j}{m_i + m_j}} \tag{8}$$

where r_i, ν_i, E_i, G_i, and ε = radius, Poisson's ratio, Young's modulus, modulus of rigidity, and restitution coefficient of the particle, respectively. The torque $\boldsymbol{M_{ij}}$ in Eq. (2) is calculated using $\boldsymbol{F_{nij}}$ as represented by Eq. (9). In addition the rolling friction $\boldsymbol{M_{rij}}$ in Eq. (10) is also considered

$$\boldsymbol{M_{ij}} = r_i \boldsymbol{n_{ij}} \times \boldsymbol{F_{nij}} \tag{9}$$

$$\boldsymbol{M_{rij}} = -\mu_r k_{nij}\delta_{nij}^{\frac{3}{2}}\frac{r_i r_j}{(r_i + r_j)}\frac{\boldsymbol{\omega_{ij}}}{|\boldsymbol{\omega_{ij}}|} \tag{10}$$

where $\boldsymbol{\omega_{ij}}$ and μ_r = relative angular velocity between particles i and j and the coefficient of rotational friction, respectively. The calculation parameters are listed in Table 1. Mechanical properties of the sample cell and the tube are set at the same parameters as those of the particle in this calculation.

Table 1. Calculation parameters for three-dimensional DEM simulation

Parameters	Values
Specific gravity of particle	2.5
Particle radius (μm)	250
Young's modulus (MPa)	70
Poisson's ratio	0.25
Restitution coefficient	0.7
Friction coefficient	0.4
Coefficient of rotational friction	0.4

Spherical particles are randomly placed in a calculation domain ($50 \times 50 \times 235$ mm) and allowed to fall freely until they create their sediment state in the gravitational accelerations of the Earth (9.8 m/s^2) and Moon (1.6 m/s^2), respectively. The number of particles for the numerical calculations was 1,500,000. The calculation time step is fixed at 1.0 μs, and the particle data are sampled every 50 ms for all cases. The specific gravity of the particles is the same as that of the glass beads used in the experiment, whereas the particle diameter is set at 500 μm, instead of the diameters used in the experiment to deal with large calculation loads when using smaller and larger number of particles. A tube with an inner diameter, thickness, and length of 10, 1, and 150 mm, respectively, is inserted vertically into the sediment particles at a depth of approximately 40 mm and a velocity of 0.5 m/s. Then, the tube is vibrated vertically with a fixed frequency of 20 Hz and at different vibration accelerations for 10 s. At the end of the calculation, the positions of particles located at the top surface of the bulk of the particles in the tube are detected, and the top planes of particles climbing are calculated from their detected positions using a least-square method. Then, the distance between the bottom of the tube and the top plane is assumed as the height in the calculation.

Results and Discussion

Transient Characteristics

Fig. 4 shows the measured lifted height of the glass beads in the tube after the application of vertical vibration. The lifted height is the distance from the surface of the regolith layer outside the tube to

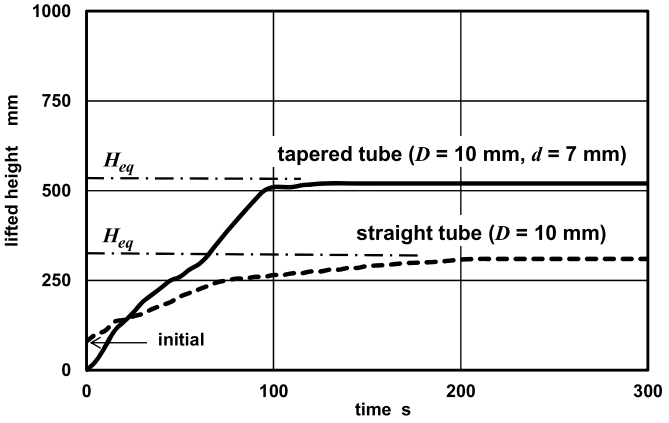

Fig. 4. Measured lifted height of glass beads in tube versus time after the application of vertical vibration ($a = 2.5$ mm, lowering speed: 575 mm/s, and lifting speed: 338 mm/s, without the application of horizontal vibration). Operational scheme on the lowering and lifting speeds is described in Fig. 10.

the top of the lifted particles in the tube, as shown in Fig. 1(b). When the straight tube was used, the tube was initially filled with particles before vertical vibration was applied. To operate the straight tube, it is crucial to carry out this procedure as reported in the literature (Liu et al. 2013; Zhang et al. 2017, 2018); however, it is not a prerequisite for the tapered tube case (Liu et al. 2014). In both the cases, particles were lifted in the tube with time, and the lifted particles in the tube finally remained at an equilibrium height H_{eq}. The equilibrium height in the tapered tube was higher than that in the straight tube, suggesting that the tapered tube is more effective for vertical transportation than the straight tube. The saturation time was approximately 100–200 s.

Effect of Vibration Acceleration

Fig. 5 shows the measured equilibrium lifted height H_{eq} of the glass beads in the tube versus the normalized acceleration G of the vertical vibration in the different tube and bead diameters. The experiment was conducted three times under the same conditions, and the averaged values were plotted in the figure. The acceleration was normalized by the gravitational acceleration g ($= 9.8$ m/s^2), i.e., $G = a(2\pi f)^2/g$, where a is the vibration amplitude and f is the frequency. Because the horizontal vibration waveform is not exactly sinusoidal, as shown in the subsequent section (Fig. 10), this definition is not thorough but provides the approximated magnitude of vibration.

The acceleration of the vibration was controlled by adjusting the vibration amplitude a of the vertical linear actuator at a constant frequency of 20 Hz. Fig. 5 shows that the lifted height increased with an increase in the amplitude of vertical vibration. This result is consistent with that reported in the literature (Liu et al. 2013, 2014; Zhang et al. 2017). Large particles in the large pipe ($D = 10$ mm) were lifted to a higher position at a relatively low acceleration than that in the small pipe ($D = 6$ mm). Therefore, it can be inferred that the large pipe is better than the small pipe for the transportation of large beads. On the contrary, a small tube is preferable for transporting small beads. An adequate combination of the tube diameter and the particle size might exist, as reported in the literature (Zhang et al. 2017; Fan et al. 2017).

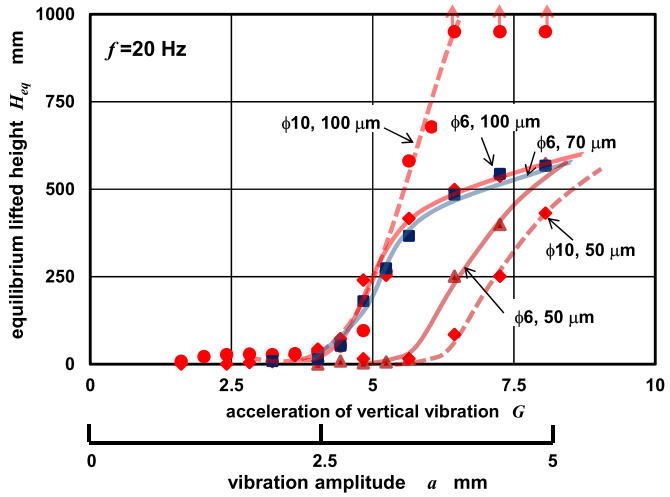

Fig. 5. Measured equilibrium lifted height of glass beads in tube versus the acceleration of vertical vibration at constant frequency (straight tube, $f = 20$ Hz, with the application of horizontal vibration). Bead diameters of 100, 70, and 50 μm designated in the figure are typical diameters of FGB-180 (106–90 μm), B-240 (75–63 μm), and FG320 (53–38 μm), respectively.

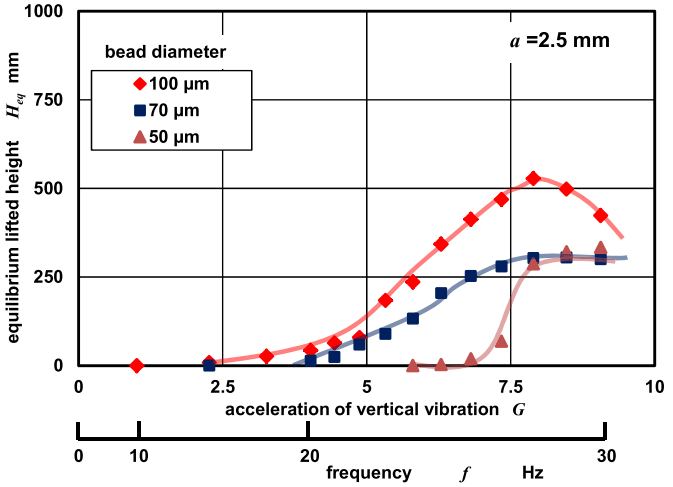

Fig. 6. Measured equilibrium lifted height of glass beads in the tube versus the acceleration of vertical vibration at constant vibration amplitude (straight tube, $D = 6$ mm, and $a = 2.5$ mm, with the application of horizontal vibration). The bead diameters of 100, 70, and 50 μm designated in the figure are typical diameters of FGB-180 (106–90 μm), B-240 (75–63 μm), and FG320 (53–38 μm), respectively.

Fig. 6 also shows the measured equilibrium lifted height versus the acceleration of vertical vibration. In this case, the acceleration was controlled by adjusting the frequency at a constant vibration amplitude of 2.5 mm. This characteristic was similar to that of the constant-frequency case; however, the lifted height did not monotonically increase as the frequency increased. Based on a void-filling model (Zhang et al. 2018), particles in the pipe are compacted and loosened alternately during vibration. The model insists that a void formed under the tip of the tube after lifting the tube is filled with surrounding particles, and then these particles are lifted when the tube is inserted, thus resulting in particle climbing. In the high-frequency case, the particles are not given enough time to move into the void. Therefore, an optimal frequency exists for the vertical transportation.

Effect of Tube Insertion Depth

Fig. 7 shows the measured equilibrium lifted height of the lunar regolith simulant in the tube versus the depth of the tube insertion. As reported in the literature (Liu et al. 2013, 2014; Zhang et al. 2017), to lift particles, the straight tube must be initially filled with particles at a certain height. This height was approximately 75 mm when the container did not vibrate horizontally. It was reduced to approximately 40 mm when the container vibrated horizontally. The initial filling was necessary for the straight tube even when the container was vibrated horizontally. On the contrary, efficient lifting and transportation of particles were possible without the initial filling and horizontal vibration when the hopper was attached at the lower end of the tube; thus, the tapered tube is preferable for practical use. The equilibrium lifted height in the tapered tube was approximately two times higher than that in the straight tube. It is assumed that fewer particles will drop from the tapered tube than from the straight tube.

Effect of Tube Geometry

Fig. 8 shows the effect of the tube diameter D. It is evident that the tapered tube is better than the straight tube (Liu et al. 2014) for transportation and an optimal diameter exists in both the straight

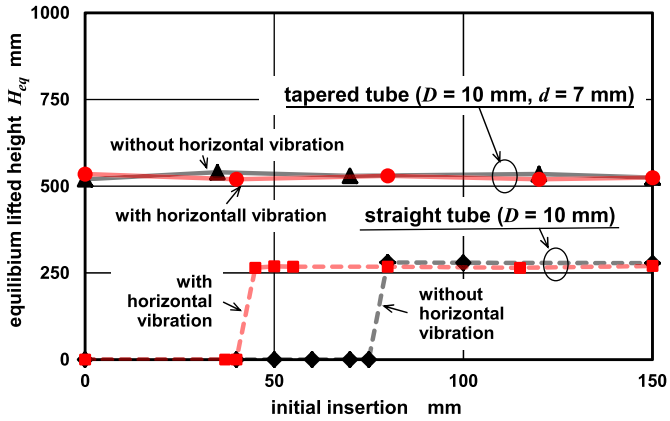

Fig. 7. Measured equilibrium lifted height in the tube versus the initial insertion depth (lunar regolith simulant, $a = 2.5$ mm, lowering speed: 575 mm/s, and lifting speed: 338 mm/s). Operational scheme of the lowering and lifting speeds is described in Fig. 10.

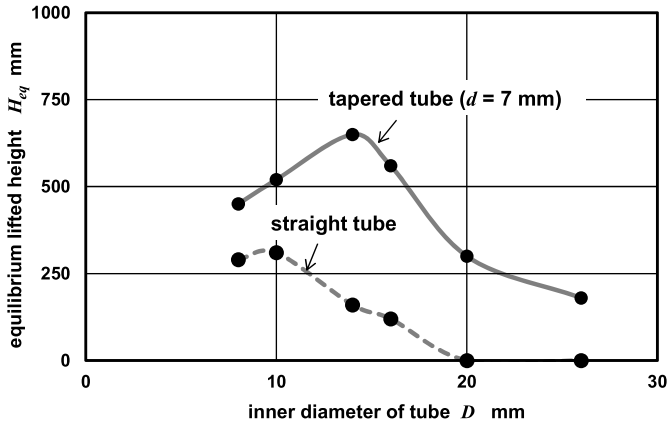

Fig. 8. Measured equilibrium lifted height in tube versus inner diameter of tube (lunar regolith simulant, $a = 2.5$ mm, lowering speed: 575 mm/s, and lifting speed: 338 mm/s, with the application of horizontal vibration). Operational scheme on the lowering and lifting speeds is described in Fig. 10.

and tapered tubes (approximately 14 mm for the tapered tube). The optimal diameter depends on the particle diameter, as discussed in the preceding section. Figs. 9(a and b) show the effect of the taper angle α and aperture of hopper $(d/D)^2$, respectively. These figures show that a small angle of approximately 10° and an aperture of 0.7 are optimal for this case.

Effect of Vibration Scheme

The waveform of the vertical vibration was not exactly sinusoidal but sawtooth like as shown in Fig. 10(a). The time lag between lifting and lowering the tube was approximately 4 ms. Here, the lifting and lowering speeds designated in the figure were varied independently to investigate the effect of the vibration scheme. The experimental results shown in Figs. 10(a and b) suggest that moderate lifting and high lowering speeds are preferable to realize a higher lifted height of particles. The void-filling model (Zhang et al. 2018) can also explain the results. The lifting speed must be moderate to fill the void formed under the tube tip.

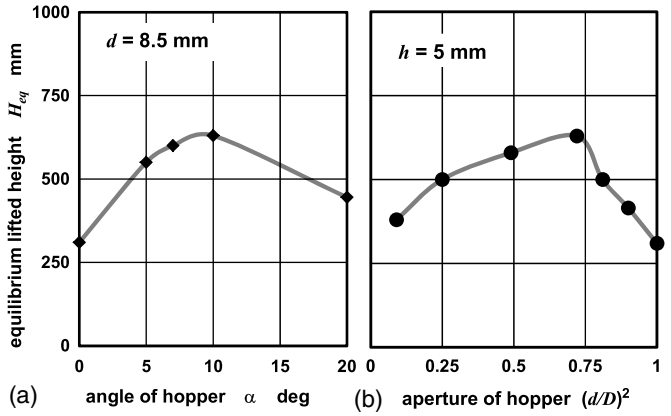

Fig. 9. Measured equilibrium lifted height in tube versus (a) angle of hopper; and (b) aperture of the tapered hopper (lunar regolith simulant, $D = 10$ mm, $a = 2.5$ mm, lowering speed: 575 mm/s, and lifting speed: 338 mm/s, without the application of horizontal vibration). Operational scheme on the lowering and lifting speeds is described in Fig. 10.

Effect of Tube Inclination

The lifted height of particles was measured when the tube was inclined. As shown in Fig. 11, it was discovered that the equilibrium lifted height was irrelevant to the inclination. The lifted height is not the length through the tube but the vertical distance from the regolith surface. The experimental result suggests that it is possible to transport particles at high positions even when the tube is inclined.

Transportation of Ice

Fig. 12 shows the measured transportation performance of ice particles mixed with lunar regolith simulant in a freezer in which the temperature was maintained at −35°C. Because the tube length was 300 mm owing to the limitation of the freezer size, the lifted height was limited to 300 mm at a water content of 5% by weight. It was demonstrated that the transportation of ice particles was successful. Although the low specific gravity of ice is advantageous for vertical transportation (Kawamoto and Yoshida 2018), frost that agglutinated the ice particles made the lifting ice particles difficult (Kawamoto et al. 2021). Moisture in the air froze in a low-temperature atmosphere, and ice particles easily adhered to each other in the container and tube. Because no moisture exists on the atmosphere of the Moon, the high transportation performance is expected against ice particles on the Moon.

Effect of Gravitational Acceleration

Here, the performance of the transportation system in the environment of the Moon is predicted by performing numerical calculations. Fig. 13(a) shows the top height of the particles in the tube with respect to time when gravitational and vibration accelerations are varied; Figs. 13(b and c) show snapshots of the initial condition and behavior of the particles climbing in the gravity of the Moon, respectively. Fig. 14 shows the lifted height at 10 s after the application of vibration in each case. The heights of the particles in the tube are approximately 40 mm as the initial condition in the Earth and Moon cases. In the case of Earth, because larger particles (500 μm in diameter) are used for calculations, they cannot climb above 10 mm in 10 s in all vibration acceleration cases and even lower in some cases, as shown in

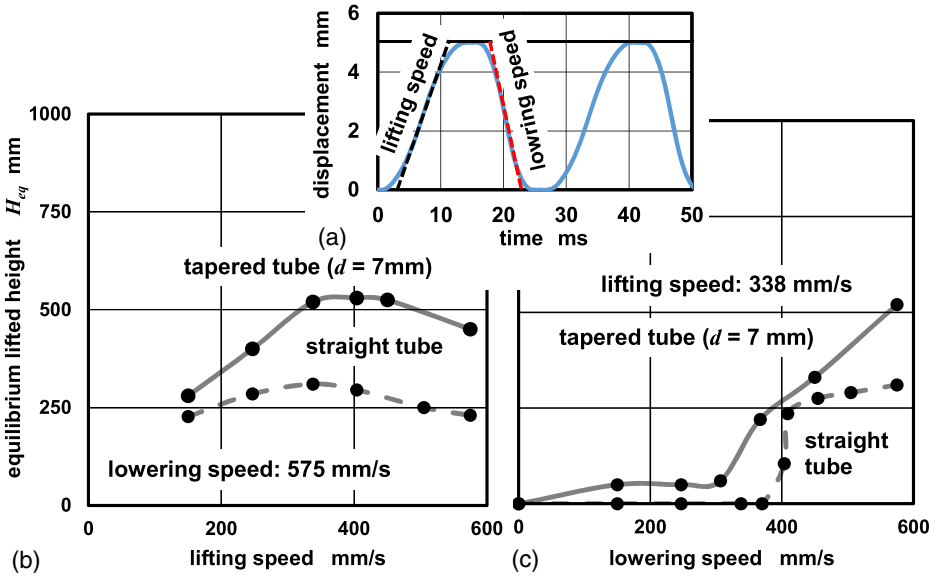

Fig. 10. (a) Measured waveform of the vertical vibration; (b) measured equilibrium lifted height of particles in the tube versus the lifting speed (lunar regolith simulant, $D = 10$ mm, $a = 2.5$ mm, and lowering speed: 575 mm/s, with the application of horizontal vibration); and (c) measured equilibrium lifted height in the tube versus the lowering speed (lunar regolith simulant, $D = 10$ mm, $a = 2.5$ mm, and lifting speed: 338 mm/s, with the application of horizontal vibration). The capacity of the linear actuator limited the speed to less than 600 mm/s.

Figs. 13(a) and 14. However, the lifted height increases with the vibration acceleration, and this trend is consistent with the experimental results.

On the other hand, the particles can climb higher in the gravity of the Moon, reaching the top of the tube in high vibration acceleration cases, as shown in Fig. 13(c). Many particles fly out of the top opening of the tube and fall, returning to the bulk of particles outside the tube. Furthermore, Fig. 13(a) shows that the climbing speed increases with an increase in the vibration acceleration on the Moon. Although the equilibrium lifted heights in the Moon cases are unknown because the tube length and calculation time are limited, it can be easily assumed that the lifted height is larger than the calculated result in Fig. 14. Thus, a lower gravitational acceleration is favorable for the vertical transportation system. Additionally, granular climbing on the Moon behaves differently from that on the Earth. The particles lifted upward in one cycle of the vibration are immediately subjected to gravity in the case of Earth, resulting in their sedimentation in the tube, whereas the lower gravitational acceleration does not largely restrict particle mobilization, allowing their flying in the tube. The granular dynamics in the Moon environment needs to be investigated in depth in future studies.

Conclusion

The development of a vertical transportation technology is crucial for the exploration of ice under the deep portion of the lunar ground. To this end, a vertical transportation system for lunar regolith and ice particles has been developed using a vertical vibration transportation mechanism. The proposed system has advantages, such

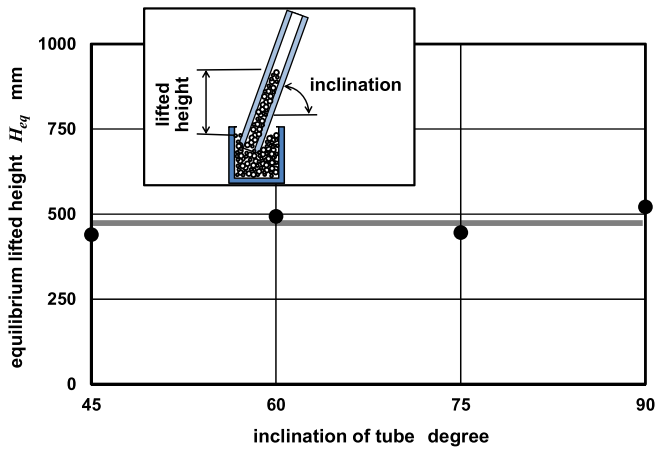

Fig. 11. Measured equilibrium lifted height in tube versus inclination of tube (lunar regolith simulant, $a = 2.5$ mm, lowering speed: 575 mm/s, and lifting speed: 338 mm/s, with the application of horizontal vibration).

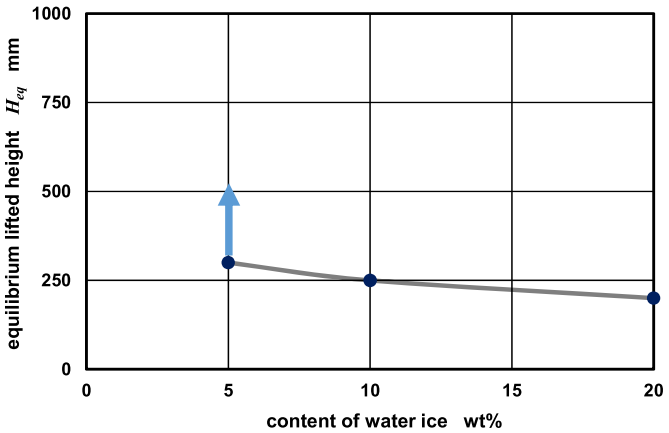

Fig. 12. Measured equilibrium lifted height in tube versus content of water ice (straight tube, $D = 10$ mm, $a = 2.5$ mm, lifting speed: 338 mm/s, lowering speed: 575 mm/s, and initial insertion depth = 50 mm, with the application of horizontal vibration).

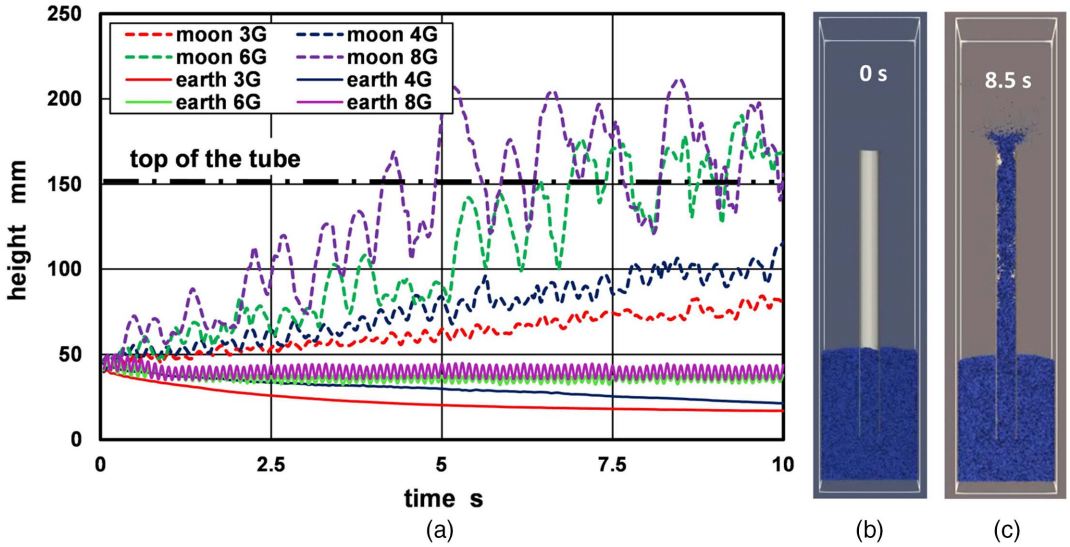

Fig. 13. (a) Calculated lifted height of particles in tube with respect to time after the application of vertical vibration when vibration and gravitational accelerations are varied; snapshots of particles (b) at initial condition; and (c) during climbing (at 8.5 s) in the case of the Moon gravity and vibration acceleration of $8g$ ($f = 20$ Hz).

as transporting particles to a higher position, easy control system, and simple structure. The following points have been clarified and demonstrated:

- Particles are collected and lifted with time in the tube by the up and down oscillation of the tube inserted vertically into the bulk of the regolith, and finally remain in the tube at an equilibrium height. The equilibrium height increases with the amplitude of vibration.
- If the lower end of the tube is straight, it must be initially filled with particles. The initial filling depth can be reduced if the particle container is vibrated horizontally.
- If the lower end of the tube has a tapered shape, the initial filling and horizontal vibration are not required. The equilibrium height in the tapered tube is higher than that in the straight tube; thus, the tapered tube is preferable for practical use.

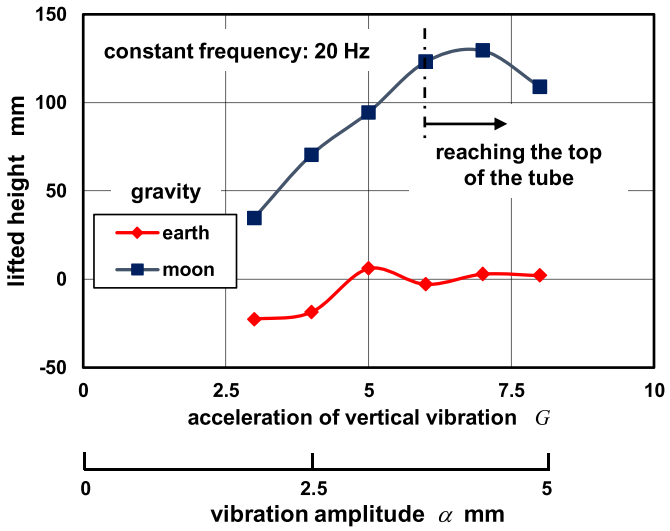

Fig. 14. Calculated lifted height of particles in the tube at 10 s versus the acceleration of vertical vibration at constant frequency in Earth and Moon gravities ($f = 20$ Hz).

- The pipe with a larger diameter is preferred for transporting large particles, whereas a tube with a small diameter is preferred for transporting small particles. An adequate combination of the tube diameter and size of particle might exist. The optimal diameter of the tube was 14 mm for the lunar regolith
- The optimal taper angle and aperture of the tapered tube were approximately 10° and 0.7, respectively.
- It is preferable to operate the system with a moderate lifting speed (approximately 400 mm/s) and a high lowering speed (higher than 500 mm/s) of the tube.
- The system can transport particles to high position even when the tube is inclined.
- Crushed ice mixed with regolith particles can be transported; however, ice particles adhere and aggregate easily owing to the frost of moisture in the low-temperature atmosphere on Earth. This unfavorable effect should be negligible in the vacuum environment on the Moon.
- The performance of transportation system, in terms of lifted height and speed of transportation, is improved on the Moon owing to its lower gravitational acceleration.

Additional research will be needed using more realistic crushed regolith to match lunar soil in vacuum and in a reduced gravity environment.

Data Availability Statement

Some data and models used during the study are available from the corresponding author by request: data in Figs. 4–13.

Acknowledgments

The authors gratefully acknowledge Kazuhiro Hata (Waseda University) for his assistance in carrying out the experiment as well as Matthias Sperl (DLR) for his support of setting up the numerical calculations. This research was supported, in part, by JSPS KAKENHI Grant Nos. 17K06276 and 20K04927, and Masato Adachi is supported by JSPS Overseas Research Fellowships and Alexander von Humboldt Research Fellowship.

Supplemental Materials

Videos S1 and S2 are available online in the ASCE Library (www.ascelibrary.org).

References

Abbey, W., et al. 2019. "A look back: The drilling campaign of the Curiosity Rover during the Mars Science Laboratory's Prime Mission." *Icarus* 319 (Feb): 1–13. https://doi.org/10.1016/j.icarus.2018.09.004.

Akiyama, T., and T. Shimomura. 1991. "Investigation of wall shear stress in vibrating particle beds." *Powder Technol.* 66 (3): 243–247. https://doi.org/10.1016/0032-5910(91)80037-J.

Allton, J. H. 2009. "Lunar samples: Apollo collection tools, curation handling, Surveyor III and Soviet luna samples." In *Proc., Lunar Regolith Simulant Workshop*. Huntsville, AL: NASA Marshall Space Flight Center.

Bonitz, R., L. Shiraishi, M. Robinson, J. Carsten, R. Volpe, A. Trebi-Ollennu, R. E. Arvidson, P. C. Chu, J. J. Wilson, and K. R. Davis. 2009. "The Phoenix Mars Lander robotic arm." In *Proc., IEEE Aerospace Conf.* New York: IEEE.

Colaprete, A., et al. 2010. "Detection of water in the LCROSS ejecta plume." *Science* 330 (6003): 463–468. https://doi.org/10.1126/science.1186986.

Cundall, P. A., and O. D. L. Strack. 1979. "A discrete numerical model for granular assemblies." *Géotechnique* 29 (1): 47–65. https://doi.org/10.1680/geot.1979.29.1.47.

Fan, S., E. J. R. Parteli, and T. Poschel. 2017. "Origin of granular capillarity revealed by particle-based simulations." *Phys. Rev. Lett.* 118 (21): 218001. https://doi.org/10.1103/PhysRevLett.118.218001.

Hoshino, T., et al. 2019. "Study status of Japanese lunar polar exploration mission." In *Proc., 32th Int. Symp. on Space Technology and Science*. Fukui, Japan: International Symposium on Space Technology and Science Organizing Committee.

Kanamori, H., S. Udagawa, T. Yoshida, S. Matsumoto, and K. Takagi. 1998. "Properties of lunar soil simulant manufactured in Japan." In *Proc., 6th Int. Conf. on Engineering, Construction and Operations in Space*, 462–468. Reston, VA: ASCE.

Kawamoto, H. 2014. "Sampling of small regolith particles from asteroids utilizing an alternative electrostatic field and electrostatic traveling wave." *J. Aerosp. Eng.* 27 (3): 631–635. https://doi.org/10.1061/(ASCE)AS.1943-5525.0000287.

Kawamoto, H., K. Hata, and T. Shibata. 2021. "Vertical transport of lunar regolith and ice particles using electrodynamic travelling-wave." *J. Aerosp. Eng.* 34 (4): 04021042. https://doi.org/10.1061/(ASCE)AS.1943-5525.0001297.

Kawamoto, H., A. Shigeta, and M. Adachi. 2016. "Utilizing electrostatic force and mechanical vibration to obtain regolith sample from the Moon and Mars." *J. Aerosp. Eng.* 29 (1): 04015031. https://doi.org/10.1061/(ASCE)AS.1943-5525.0000521.

Kawamoto, H., and K. Shirai. 2012. "Electrostatic transport of lunar soil for in situ resource utilization." *J. Aerosp. Eng.* 25 (1): 132–138. https://doi.org/10.1061/(ASCE)AS.1943-5525.0000094.

Kawamoto, H., and N. Yoshida. 2018. "Electrostatic sampling and transport of ice for in-situ resource utilization." *J. Aerosp. Eng.* 31 (4): 04018044. https://doi.org/10.1061/(ASCE)AS.1943-5525.0000866.

Klein, H. P., J. Lederberg, A. Rich, N. H. Horowitz, V. I. Oyama, and G. V. Levin. 1976. "The Viking mission and the search for life on Mars." *Nature* 262: 24–27. https://doi.org/10.1038/262024a0.

Kloss, C., C. Goniva, A. Hager, S. Amberger, and S. Pirker. 2012. "Models, algorithms and validation for opensource DEM and CFD-DEM." *Prog. Comput. Fluid Dyn. Int. J.* 12 (2–3): 140–152. https://doi.org/10.1504/PCFD.2012.047457.

Lee, K. A., L. Oryshchyn, A. Paz, M. Reddington, and T. M. Simon. 2013. "The ROxygen project: Outpost-scale lunar oxygen production system development at Johnson Space Center." *J. Aerosp. Eng.* 26 (1): 67–73. https://doi.org/10.1061/(ASCE)AS.1943-5525.0000230.

Li, S., P. G. Lucey, R. H. Milliken, P. O. Hayne, E. Fisher, J.-P. Williams, D. M. Hurley, and R. C. Elphic. 2018. "Direct evidence of surface exposed water ice in the lunar polar regions." *Proc. Natl. Acad. Sci.* 115 (36): 8907–8912. https://doi.org/10.1073/pnas.1802345115.

Liu, C., P. Wu, and L. Wang. 2013. "Particle climbing along a vibrating tube: A vibrating tube that acts as a pump for lifting granular materials from a silo." *Soft Matter* 9 (19): 4762–4766. https://doi.org/10.1039/c3sm27955c.

Liu, C., F. Zhang, P. Wu, and Li Wang. 2014. "Effect of hoisting tube shape on particle climbing." *Powder Technol.* 259 (Jun): 137–143. https://doi.org/10.1016/j.powtec.2014.03.056.

Lucey, P. G. 2009. "A lunar waterworld." *Science* 326 (5952): 531–532. https://doi.org/10.1126/science.1181471.

McKay, D. S., G. H. Heiken, A. Basu, G. Blanford, S. Simon, R. Reedy, B. M. French, and J. Papike. 1991. "The lunar regolith." In *Lunar sourcebook*, edited by G. Heiken, D. Vaniman, and B. M. French, 285–356. Cambridge, UK: Cambridge University Press.

Ohtsuki, T., D. Kinoshita, Y. Nakada, and A. Hayashi. 1998. "Surface level mitigation in vibrating beds of cohesionless granular materials." *Phys. Rev. E* 58 (6): 7650–7656. https://doi.org/10.1103/PhysRevE.58.7650.

Sanders, G. B., and W. E. Larson. 2011. "Integration of in-situ resource utilization into lunar/Mars exploration through field analogs." *Adv. Space Res.* 47 (1): 20–29. https://doi.org/10.1016/j.asr.2010.08.020.

Sanders, G. B., and W. E. Larson. 2013. "Progress made in lunar in situ resource utilization under NASA's exploration technology and development program." *J. Aerosp. Eng.* 26 (1): 5–17. https://doi.org/10.1061/(ASCE)AS.1943-5525.0000208.

Sanin, A. B., et al. 2017. "Hydrogen distribution in the lunar polar regions." *Icarus* 283 (Feb): 20–30. https://doi.org/10.1016/j.icarus.2016.06.002.

Wakabayashi, S., Y. Shirasawa, and T. Hoshino. 2019. "Japanese lunar polar exploration mission: Status of rover system study." In *Proc., 32th Int. Symp. on Space Technology and Science*. Fukui, Japan: International Symposium on Space Technology and Science Organizing Committee.

Zacny, K., et al. 2013. "Lunar Vader: Development and testing of lunar drill in vacuum chamber and in lunar analog site of Antarctica." *J. Aerosp. Eng.* 26 (1): 74–86. https://doi.org/10.1061/(ASCE)AS.1943-5525.0000212.

Zhang, F., K. Cronin, Y. Lin, C. Liu, and L. Wang. 2018. "Effects of vibration parameters and pipe insertion depth on the motion of particles induced by vertical vibration." *Powder Technol.* 333 (Jun): 421–428. https://doi.org/10.1016/j.powtec.2018.04.066.

Zhang, F., L. Wang, C. Liu, and P. Wu. 2017. "Climbing motion of grains in vibrating tubes with different geometries." *Adv. Powder Technol.* 28 (2): 356–362. https://doi.org/10.1016/j.apt.2016.09.027.